Department of Signal Processing and Acoustics

Characterization of Light Emitting Diodes and Photometer Quality Factors

Tuomas Poikonen

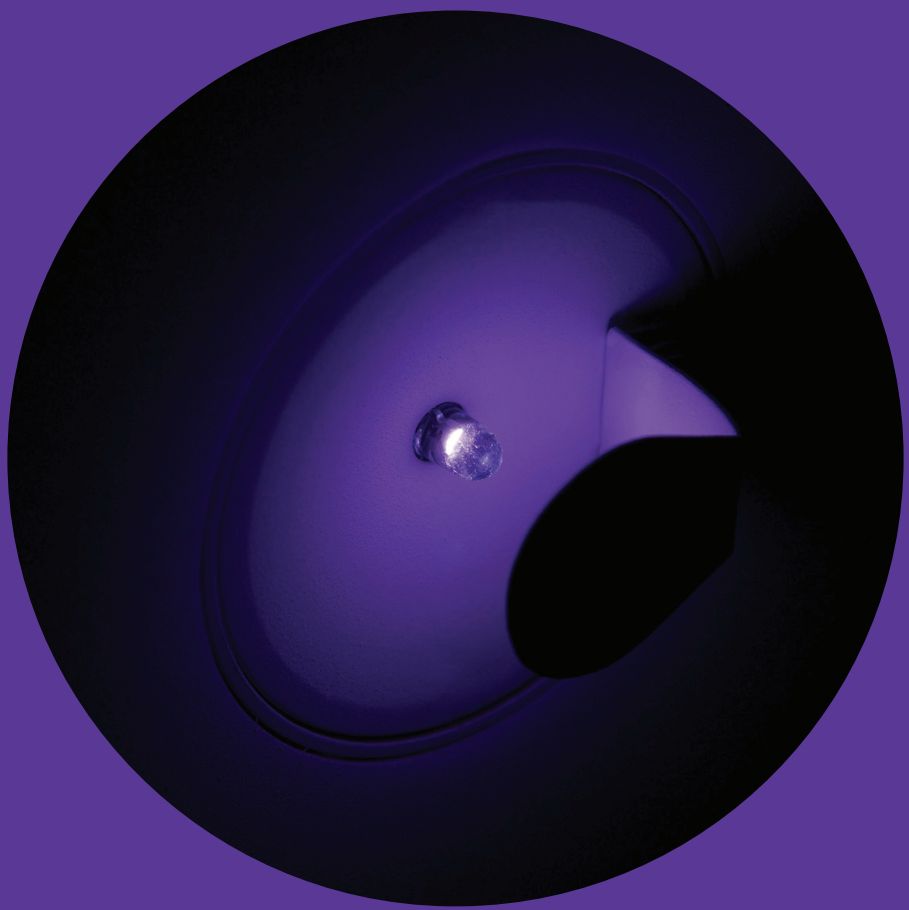

Aalto University

DOCTORAL DISSERTATIONS

Aalto University publication series
DOCTORAL DISSERTATIONS 165/2012

Characterization of Light Emitting Diodes and Photometer Quality Factors

Tuomas Poikonen

A doctoral dissertation completed for the degree of Doctor of Science (Technology) to be defended, with the permission of the Aalto University School of Electrical Engineering, at a public examination held at the lecture hall S2 of the school on 7 December 2012 at 12.

Aalto University
School of Electrical Engineering
Department of Signal Processing and Acoustics
Metrology Research Institute

Supervising professor
Prof. Erkki Ikonen

Thesis advisor
Doc. Petri Kärhä

Preliminary examiners
Dr. John Clare, Measurement Standards Laboratory, New Zealand
Dr. Jarle Gran, Justervesenet, Norway

Opponent
Dr. Armin Sperling, Physikalisch-Technische Bundesanstalt, Germany

Aalto University publication series
DOCTORAL DISSERTATIONS 165/2012

ISBN 978-952-60-4901-4 (printed)
ISBN 978-952-60-4902-1 (pdf)
ISSN-L 1799-4934
ISSN 1799-4934 (printed)
ISSN 1799-4942 (pdf)
http://urn.fi/URN:ISBN:978-952-60-4902-1

Unigrafia Oy
Helsinki 2012

Finland

441 697
Printed matter

Author
Tuomas Poikonen

Name of the doctoral dissertation
Characterization of Light Emitting Diodes and Photometer Quality Factors

Publisher School of Electrical Engineering

Unit Department of Signal Processing and Acoustics

Series Aalto University publication series DOCTORAL DISSERTATIONS 165/2012

Field of research Measurement Science and Technology

Manuscript submitted 17 September 2012 **Date of the defence** 7 December 2012

Permission to publish granted (date) 5 November 2012 **Language** English

☐ **Monograph** ☒ **Article dissertation (summary + original articles)**

Abstract

Light-emitting diodes (LEDs) are used in various applications due to their small size, durability and energy efficiency. The introduction of white high-brightness LEDs has changed the lighting, electronics and automobile industries for good. Incandescent lamps are being replaced by solid-state lamps (SSLs) for better energy efficiency. However, the optical and electrical properties of LEDs and SSLs differ from incandescent lamps, and characterization of these new light sources requires careful evaluation of the measurement methods for obtaining low measurement uncertainty. In this thesis, measurement setups have been developed for luminous flux and luminous efficacy measurements of LEDs and SSLs. The photometer heads utilized in the measurements have been characterized for the spectral and directional responses. Methods for analyzing the uncertainties of the photometer spectral and directional quality indices f_1' and f_2 have been developed using Monte Carlo simulation.

A multifunctional 30-cm integrating sphere has been constructed with custom ports and baffles for total and partial luminous flux measurements of both low- and high-power LEDs. The spatial corrections obtained are less than 0.2 % for typical directional LEDs. The expanded uncertainty ($k = 2$) of the measurement setup varies between 1.2 % and 4.6 %, depending on the color and the angular spread of the LED. For luminous efficacy measurements of SSLs, a measurement setup based on a compact goniospectrometer and a 1.65-m integrating sphere has been constructed. Test measurements of 25 different SSLs showed large differences between the lamps, especially in the luminous efficacies and the quality of the built-in power supplies. It was also found that the self-absorptions of SSLs have spectral dependence due to the materials used in the lamps. The luminous efficacy of a typical SSL with stable electronics can be measured with 1.2 % ($k = 2$) expanded uncertainty.

The uncertainties of the spectral and directional quality indices f_1' and f_2 of photometers have been investigated using Monte Carlo simulation with biased and random error models. The results show that simple random variation of the individual data points of the response data may lead to underestimated uncertainty of the quality index. For proper estimation of the uncertainties, physical models of the characterization measurements are needed. The developed methods give, for the first time, a solid basis for the uncertainty analysis of the photometer quality indices, which manufacturers typically report without uncertainties.

Keywords Photometry, integrating sphere, goniometer, photometer, light-emitting diode, solid-state lighting, luminous flux, electrical power, luminous efficacy, spectral responsivity, directional response, quality index

ISBN (printed) 978-952-60-4901-4 **ISBN (pdf)** 978-952-60-4902-1

ISSN-L 1799-4934 **ISSN (printed)** 1799-4934 **ISSN (pdf)** 1799-4942

Location of publisher Espoo **Location of printing** Helsinki **Year** 2012

Pages 92 **urn** http://urn.fi/URN:ISBN:978-952-60-4902-1

Tekijä
Tuomas Poikonen

Väitöskirjan nimi
Loistediodien ja fotometrien hyvyyslukujen karakterisoinnit

Julkaisija Sähkötekniikan korkeakoulu

Yksikkö Signaalinkäsittelyn ja akustiikan laitos

Sarja Aalto University publication series DOCTORAL DISSERTATIONS 165/2012

Tutkimusala Mittaustekniikka

Käsikirjoituksen pvm 17.09.2012 **Väitöspäivä** 07.12.2012

Julkaisuluvan myöntämispäivä 05.11.2012 **Kieli** Englanti

☐ **Monografia** ☒ **Yhdistelmäväitöskirja (yhteenveto-osa + erillisartikkelit)**

Tiivistelmä

Loistediodeja (LEDejä) käytetään useissa sovelluksissa niiden pienen koon, kestävyyden ja hyvän energiatehokkuuden vuoksi. Valkoisten kirkkaiden LEDien tultua saataville valaistus-, elektroniikka- ja autoteollisuus ovat kokeneet suuren muutoksen. Yleiskäytössä olevat hehkulamput tullaan syrjäyttämään uusilla LED-pohjaisilla ratkaisuilla. LEDien ja LED-pohjaisten energiansäästölamppujen optiset ja sähköiset ominaisuudet poikkeavat hehkulamppujen ominaisuuksista kuitenkin merkittävästi. Pienten mittausepävarmuuksien saavuttamiseksi LEDeihin liittyvät fotometriset mittausmenetelmät tulee arvioida huolellisesti. Tässä työssä on kehitetty mittauslaitteistot LEDien ja LED-pohjaisten energiansäästölamppujen valovirran ja valotehokkuuden mittaamista varten. Mittauksissa käytettävien fotometrien spektristen herkkyyksien ja kosinivasteiden karakterisointien pohjalta on lisäksi kehitetty menetelmät fotometrien hyvyyslukujen f_1' ja f_2 epävarmuuksien analysointia varten käyttäen Monte Carlo-simulaatiota.

Työssä on kehitetty pien- ja suurteho-LEDien valovirran mittaamiseen monikäyttöinen mittauslaitteisto, joka perustuu 30-cm erikoisrakenteiseen integroivaan palloon. Laitteistolla saavutettavat spatiaalikorjaukset ovat suuruudeltaan alle 0.2 % mitattaessa tyypillisiä suuntaavia LEDejä. Riippuen tutkittavan LEDin väristä ja valokeilan leveydestä, mitatun valovirran laajennettu epävarmuus (k = 2) on 1,2 – 4,6 %. LED-pohjaisten energiansäästölamppujen valotehokkuusmittauksia varten on kehitetty mittauslaitteisto, joka perustuu kompaktiin goniospektrometriin ja 1.65-m integroivaan palloon. Tutkimuksessa käytettyjen kaupoissa myytävien LED-lamppujen mittaustuloksissa havaittiin huomattavia eroja valotehokkuuksissa ja sisäänrakennettujen teholähteiden laadussa. Tulokset osoittavat myös, että LED-lampuissa käytettävät materiaalit aiheuttavat lamppujen itseabsorptioihin spektristä riipppuvuutta. Mittalaitteistolla voidaan mitata stabiilin LED-pohjaisen energiansäästölampun valotehokkuus 1.2 % (k = 2) laajennetulla epävarmuudella.

Fotometrien spektrisen herkkyyden ja kosinivasteen sovituksen laatua kuvaavien hyvyyslukujen f_1' ja f_2 epävarmuuksia on tutkittu Monte Carlo-simulaatiolla. Tutkimuksessa vertailtiin satunnaisten ja biasoitujen virhemallien soveltuvuutta epävarmuuden simulointiin. Tulosten perusteella mittapisteiden satunnainen poikkeutus tuottaa aliarvioidun epävarmuuden hyvyysluvuille. Hyvyyslukujen todellisten epävarmuuksien simulointi vaatii mittauksiin pohjautuvien virhemallien käyttöä. Fotometrien valmistajat ovat perinteisesti ilmoittaneet hyvyysluvut ilman epävarmuuksia. Tutkimuksessa kehitetyt menetelmät antavat ensimmäistä kertaa vahvan pohjan fotometrien hyvyyslukujen epävarmuuden analysoinnille.

Avainsanat Fotometria, integroiva pallo, goniometri, fotometri, loistediodi, valovirta, sähköteho, valotehokkuus, spektrinen herkkyys, kosinivaste, hyvyysluku

ISBN (painettu) 978-952-60-4901-4 **ISBN (pdf)** 978-952-60-4902-1

ISSN-L 1799-4934 **ISSN (painettu)** 1799-4934 **ISSN (pdf)** 1799-4942

Julkaisupaikka Espoo **Painopaikka** Helsinki **Vuosi** 2012

Sivumäärä 92 **urn** http://urn.fi/URN:ISBN:978-952-60-4902-1

Preface

The work of this thesis was carried out at the Metrology Research Institute of Aalto University during 2007 – 2012. I want to thank the head of the laboratory, Professor Erkki Ikonen for the opportunity to work in research projects involving light-emitting diodes and solid-state lighting.

I am grateful to my instructors Doc. Petri Kärhä and Dr. Pasi Manninen for their guidance and advice during the years. I express my gratitude to all co-authors of the publications, and colleagues at the Metrology Research Institute. Mr. Seppo Metsälä deserves special thanks for machining of high quality parts for the research.

I wish to thank the preliminary examiners Dr. John Clare and Dr. Jarle Gran for their efforts. The Finnish Foundation for Technology Promotion is acknowledged for the financial support of the research. Finally, I want to thank my parents and friends for their support.

Espoo, November 2012

Tuomas Poikonen

Contents

List of publications

This thesis consists of an overview and of the following publications:

I T. Poikonen, P. Manninen, P. Kärhä, and E. Ikonen, "Multifunctional Integrating Sphere Setup for Luminous Flux Measurements of Light Emitting Diodes," *Rev. Sci. Instrum.* **81**, 023102 (2010).

II T. Poikonen, T. Pulli, A. Vaskuri, H. Baumgartner, P. Kärhä, and E. Ikonen, "Luminous Efficacy Measurement of Solid-State Lamps," *Metrologia* **49**, S135–S140 (2012).

III T. Poikonen, P. Kärhä, P. Manninen, F. Manoocheri, and E. Ikonen, "Uncertainty Analysis of Photometer Quality Factor f_1'," *Metrologia* **46**, 75–80 (2009).

IV T. Poikonen, P. Blattner, P. Kärhä, and E. Ikonen, "Uncertainty Analysis of Photometer Directional Response Index f_2 using Monte Carlo Simulation," *Metrologia* **49**, 727–736 (2012).

Author's contribution

The publications of this thesis are products of joint work of the authors.

For publication I, the author designed and constructed the measurement setup, and conducted the characterization measurements and data analysis.

For publication II, the author prepared the measurement procedure, supervised a research team, and conducted part of the measurements and data analysis.

For publication III, the author measured spectral responsivities of two photometers, wrote a simulation software, and analyzed the data.

For publication IV, the author measured directional responses of three photometers, derived uncertainty models for the measurement, wrote a simulation software, and analyzed the data.

All manuscripts were written by the author.

Symbols and abbreviations

d	Distance
d_o	Diffuser offset
f_1'	Photometer spectral quality index
f_2	Photometer directional quality index
k	Coverage factor
$R(\varepsilon,\varphi)$	Photometer directional response
$S_A(\lambda)$	Spectrum of CIE standard illuminant A
$s_{rel}(\lambda)$	Relative spectral responsivity
$s^*_{rel}(\lambda)$	Normalized relative spectral responsivity
$V(\lambda)$	Luminous sensitivity of human eye
x	Opening angle
ε	Angle of rotation
φ	Azimuth angle

AC	Alternating current
$BaSO_4$	Barium sulfate
CCT	Correlated color temperature
CFL	Compact fluorescent lamp
CIE	International Commission on Illumination
DC	Direct current
E27	27-mm Edison screw-base
LED	Light-emitting diode
PSU	Power supply
SRDF	Spatial response distribution function
SSL	Solid-state lamp
THD	Total harmonic distortion

1. Introduction

1.1 Background

Light-emitting diodes (LEDs) have been utilized in electronic equipment as indicator lights for decades due to their small size, durability and energy efficiency. However, development of the blue high-brightness LEDs and white phosphor-coated LEDs has brought the electronics, lighting and automotive industries to a new era [1-4]. White LEDs are used in display backlights, car headlights, camera flashes of mobile phones, as well as in general lighting. LEDs offer a vast amount of new possibilities for product design, as compared to the traditional light sources [5].

However, the optical properties of LEDs are more complex than those of incandescent lamps. The luminous intensity and spectral power distribution of LEDs are sensitive to the variations in the junction temperature [6]. LEDs are available in various types of packaging, designed for different kinds of applications. The packaging directly affects the optical properties of the LED, especially the angular intensity distribution [7-10]. A typical radiation pattern of an LED is between Lambertian and highly directional [8-10]. Many low-power LEDs emit light also backwards due to the construction of their epoxy lens. LEDs with specially tuned angular distributions, such as side-emitting LEDs, are useful when the application does not allow room for any additional optical components. Due to the manufacturing tolerances, LEDs are binned according to their properties, such as luminous intensity and chromaticity values [11].

Two important photometric quantities involved in the development of energy efficient lighting and tuning of the performance of high-brightness LEDs are the luminous flux and luminous efficacy. The luminous flux in units of lumen (lm) corresponds to the total optical power emitted by the light source, weighted by the $V(\lambda)$-function that describes the spectral sensitivity of the human eye [12,13]. The luminous efficacy in units of lm/W is the measure of the energy efficiency of the light source, and is obtained by measuring the electrical power consumption of the light source in addition to its luminous flux [12,14]. Although LEDs bring new possibilities to the product development, they also bring challenges in the optical measurements needed for characterizing their performance. Because the optical properties of LEDs differ from those of incandescent lamps, traditional measurement methods may not be applicable. The methods

originally developed for incandescent lamps may need to be modified or completely redesigned in order to be compatible with LEDs [15-23].

European Commission announced in 2009 that general purpose incandescent lamps are phased out in Europe gradually before the end of September 2012 due to their poor energy efficiency [24]. Typical light bulbs used for general lighting need to be replaced by energy-saving lamps. The luminous efficacy of a typical incandescent lamp is limited to about 17 lm/W, whereas compact fluorescent lamps can reach luminous efficacies up to 90 lm/W [5]. However, solid-state lamps and luminaires (SSLs) based on LEDs have recently become even more popular. They offer longer lifetime and have potential to provide luminous efficacies higher than 100 lm/W [4,5]. In addition, SSLs are environmentally safe as compared to CFLs that contain mercury [5].

The transition from incandescent lamps and CFLs to SSLs has been made easier for the consumers by introducing a variety of SSLs that can be retrofitted to the existing E27-base [25]. Although these lamps do not necessarily produce the same luminous efficacy values or have the other benefits of a complete SSL luminaire designed for a particular application, they can be instantly used nearly anywhere due to the E27-base. Although very high values of luminous efficacy are reported for single LED-components [5], the efficacy of the final product, a lamp or a luminaire, is heavily affected by the efficiency of the built-in power supply (PSU), optics and the thermal management of the product [25-28]. Yet another thing to consider is that although the lifetime of the LED-components can be several years, it can be drastically limited by the quality of the built-in PSU [29-32].

In order to measure the photometric properties of LEDs and SSLs with low uncertainty, the equipment used for the measurements needs to be carefully characterized. Luminous flux measurements of light sources are often carried out using an integrating sphere and a photometer head for recording the illuminance level inside the sphere [8,13]. The photometer head should have spectral responsivity close to the $V(\lambda)$ and a directional response close to the ideal cosine-function. The $V(\lambda)$-matching is achieved using optical filters, and the cosine response is obtained using a diffuser at the input of the photometer. Manufacturers use quality indices for reporting the performance of photometers. The directional and spectral quality indices f_1' and f_2 describe the quality of the matching of the photometer response with the $V(\lambda)$ and cosine functions, respectively [33].

Although the quality indices cannot be used for applying a correction for the measured values, lower measurement uncertainties can be obtained with a good quality photometer head due to smaller correction factors needed.

Although the quality indices of photometers have been in use for years, they are typically reported without uncertainties, because no method has been generally accepted for determining the uncertainties. This arises a problem that if the uncertainties of the quality indices are not reported, how can one trust them? The uncertainty analysis of f_1' and f_2 using analytical methods [34] is not straightforward, because they are defined as spectral and angular integrals and consist of several underlying uncertainties of the characterization measurements. For analyzing the uncertainties of such quality indices, statistical Monte Carlo simulation is often needed [35-38]. The method is useful for simulating complex systems with a large number of variables. However, in order to obtain reliable uncertainty estimates with the Monte Carlo simulation, proper understanding of the characterization measurements of the photometer and the underlying uncertainties is needed. Simple random variation of the data in the simulation may lead to underestimated uncertainty of the quality index [38].

1.2 Contents of the thesis

In this thesis, measurement setups are constructed and characterized for luminous flux and luminous efficacy measurements of LEDs and SSLs [I, II]. The spectral responsivities and directional responses of the photometer heads required in the measurements are characterized, and their quality indices are analyzed using Monte Carlo simulation with error models derived for the characterization measurements [III, IV].

In chapter 2, the challenges of luminous flux measurements of LEDs are discussed. Then, the measurement setup of [I] is presented. Chapter 3 discusses the luminous efficacy measurements of SSLs [II]. Chapters 4 and 5 focus on the characterizations of the photometer spectral responsivities and directional responses, and the uncertainty analysis of the quality indices f_1' and f_2 [III, IV]. The conclusions are presented in chapter 6.

1.3 Scientific contribution

The thesis contains the following new scientific results:

1. A measurement setup has been published that is capable of measuring the luminous flux of LED-components in all geometries of

CIE Publication 127 using a single 30-cm integrating sphere with highly uniform spatial uniformity. The author is not aware of any other publication where such a system is reported.

2. A measurement setup based on a 1.65-m integrating sphere and a compact goniospectrometer has been developed for luminous efficacy measurements of SSLs. It has been found that the self-absorption of LED-based lamps have spectral dependence when measuring with an integrating sphere due to the materials used in the lamps. An overview of the optical and electrical properties of typical SSLs available in the market has been published. The author is not aware of other publications that present traceable luminous efficacy measurements of SSLs.

3. A novel method for analyzing the uncertainty of the photometer spectral quality factor f_1' has been developed using Monte Carlo simulation and a biased error model based on the derivative of the photometer spectral responsivity. It has been demonstrated that a typical Monte Carlo simulation with simple random variation of the data points clearly underestimates the uncertainty of the quality factor. The developed biased error model can be used as the basis for uncertainty analysis of spectral integrals.

4. A method for analyzing the uncertainty of the photometer directional response index f_2 has been developed using Monte Carlo simulation with random and biased error models. The values of f_2 of each azimuth angle of a photometer have been found highly sensitive to the asymmetry of the photometer construction. In addition, it has been discovered that the f_2 is sensitive to the position of the axis of rotation with respect to the receiving plane of the photometer, and for any photometer, a virtual minimum value of f_2 exists. The Monte Carlo analysis of f_2 for photometric directional responses has not been published earlier.

2. Luminous Flux Measurement of Light-Emitting Diodes

International Commission on Illumination (CIE) has published recommendations for measurements of LEDs in CIE Publication 127 [8]. The luminous flux of LEDs can be measured using a goniophotometer or an integrating sphere photometer. When using a goniophotometer, a photometer head is rotated around the LED at a fixed distance and illuminance values are measured. The total luminous flux is then obtained by integrating the illuminance values over the area of the virtual surface defined by the measurement geometry. Although goniometers can provide low measurement uncertainties, they can be mechanically challenging and require long measurement times. It is possible to measure the luminous flux quicker using an integrating sphere photometer. The flux of the LED is collected using a diffuse-reflective sphere and the flux level inside the sphere is measured using a detector on the sphere wall [8]. However, due to the complex optical properties of some LEDs (see Figure 1), careful characterization of the LED and the measurement setup are required for obtaining a low measurement uncertainty [6-11].

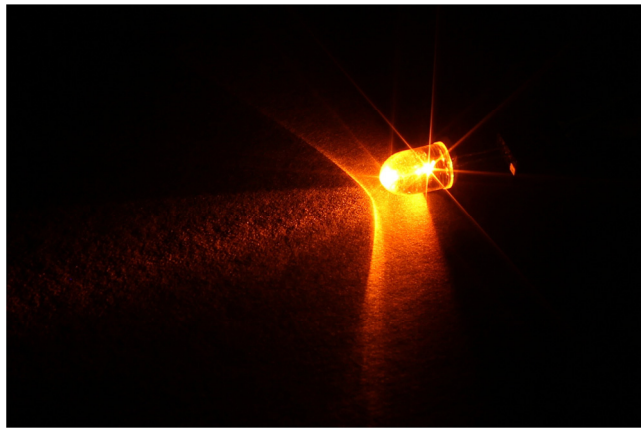

Figure 1. LED-component with complex radiation pattern.

2.1 Integrating spheres

Laboratories with photometric calibration facilities often have integrating spheres available for measurements of incandescent lamps [39–41]. The diameters of these spheres are typically in the range of 1 – 4 m. It is possible to convert such a setup for measurements of LEDs [15]. However, using a

smaller sphere for LEDs may be more convenient to avoid problems with signal-to-noise ratios, because the flux levels of LEDs are typically lower than those of incandescent lamps [19,20,23]. Integrating spheres are available for measurement of LEDs from a couple of different manufacturers. Typical sphere diameters in LED measurements vary between 0.2 – 1.0 m [19-21,23]. In addition to laboratory calibrations, integrating spheres are used for LED measurements in product development and testing, as well as in manufacturing due to the short time required by the measurement.

A typical integrating sphere designed for measurement of LEDs has ports for the LED, photometer head, and for an auxiliary lamp that is needed for the self-absorption measurement of the LED. Figure 2 shows the two total luminous flux measurement geometries recommended in [8]. LEDs with 2π radiation can be mounted on the sphere wall, while LEDs with 4π radiation need a holder. Depending on the construction of the sphere, an additional port may be needed for calibration of the sphere with an external source [19].

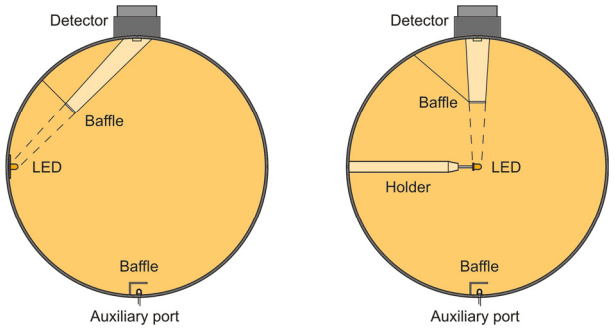

Figure 2. Total luminous flux measurement geometries for LEDs with 2π (left) and 4π (right) radiation, recommended in [8].

The sphere surface is typically coated with barium sulfate $BaSO_4$ [13]. The photometer head needs to have a good cosine response and a spectral responsivity close to the $V(\lambda)$. The direct exposure of the photometer head is blocked using a small baffle between the LED and the detector head. In addition to the two total flux geometries, the partial flux of an LED (see Figure 3) can be measured using a 50-mm entrance aperture for the LED. The distance from the tip of the LED to the aperture plane defines an opening angle x, in which the sphere collects the flux [8]. In Figure 3, only the flux drawn with color is collected by the sphere. The rest of the flux outside of the angle x is not taken into account in the measurement.

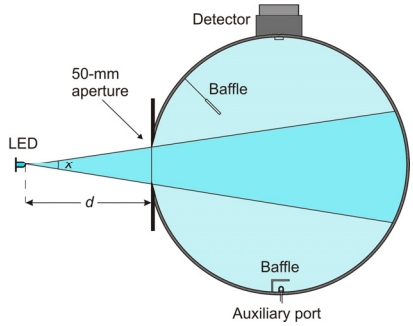

Figure 3. Partial LED flux measurement according to [8].

The luminous flux responsivity of an integrating sphere setup is typically characterized using standard LEDs [17,18,22] or an external broadband source [15,19,20,23]. When using standard LEDs, the test LED is calibrated against a standard LED of the same color and angular spread. Spectral and spatial corrections are not needed. However, using standard LEDs requires maintenance of a large number of LEDs with different colors and angular spreads. If an external incandescent source is used in the calibration, almost any kinds of LEDs can be measured, but each individual LED requires its spectral and angular properties to be measured for spectral mismatch and spatial corrections.

2.2 Challenges of flux measurements

The ports, baffles and the possible contamination of the sphere coating may cause nonuniformity in the spatial response of the sphere [39-43]. In the case of incandescent lamps, the effect of the spatial nonuniformity is often small, because the angular intensity distributions of incandescent lamps are close to isotropic [44]. However, this needs to be taken into account with LEDs, because they are often highly directional and the deviations in the sphere uniformity need to be corrected for [9,10,19,23]. Although a better signal-to-noise ratio is obtained using a smaller sphere, the baffles, ports and holders need to be made smaller too to avoid problems with the spatial nonuniformity.

The spatial correction factor can be calculated for an LED, if its angular intensity distribution is known and the spatial response distribution function (SRDF) of the sphere is measured. The angular intensity distribution of the LED can be measured using a goniophotometer [8,16,22]. In some cases, it is sufficient to use the angular data provided by the LED manufacturer. The spatial response of an integrating sphere can be determined using a sphere scanner [41–43]. However, scanning of small

integrating spheres may be challenging because sphere scanners are often designed for the E27-base, and can be of the same size as the sphere itself. It is possible to model the spatial responsivity of a sphere, but it does not reveal the nonuniformity of the coating material or its contamination [23].

In the case of low-power LEDs, part of the light is emitted backwards from the epoxy lens, and needs to be taken into account in the design of the holder for the measurements in the 4π geometry. Traditional lamp holders designed for incandescent lamps are often too large for LEDs, and can compromise the spatial response of the sphere due to screening. For measurements of LEDs, the screening of the holder should be avoided by minimizing the size of the holder [15]. LEDs can be highly sensitive to temperature changes. Because temperature control is often not implemented in the holder, the voltage of the LED needs to be measured instead [6,8,11].

High-power LEDs can produce significant amount of heat and need to be equipped with heatsinks to maintain stable operating temperature during the measurements. Measuring large LED-modules with heatsinks inside a small integrating sphere may not be practical due to high self-absorption corrections needed. An integrating hemisphere with a mirror has been proposed for measurements of high-power LED-modules. Due to the construction, the setup allows the LED-module to be mounted in the center of a virtual integrating sphere [21].

2.3 Multi-functional measurement setup

At the time of writing [I], sphere manufacturers typically offered separate products for measuring the luminous flux of LEDs in different geometries. We then decided to build a measurement setup using a single 30-cm integrating sphere with custom port and baffle design that can be configured for both low- and high-power LEDs. The functional diagram of the multifunctional measurement setup, capable of measuring the luminous flux of LEDs in all geometries of [8], is shown in Figure 4.

The coating of the sphere is $BaSO_4$ with reflectance of 97 %. The number and the area of the ports and the baffles were minimized. In addition to the detector port and the auxiliary port, the sphere has only one main port that is used for the test LED, and for the calibration of the sphere. The sphere can be quickly configured for different measurement geometries by changing the part attached to the main port of the sphere. In the detector port, a photometer head or a spectroradiometer with a diffuser

head is used for measuring the luminous flux level or the spectral power distribution of the test LED, respectively.

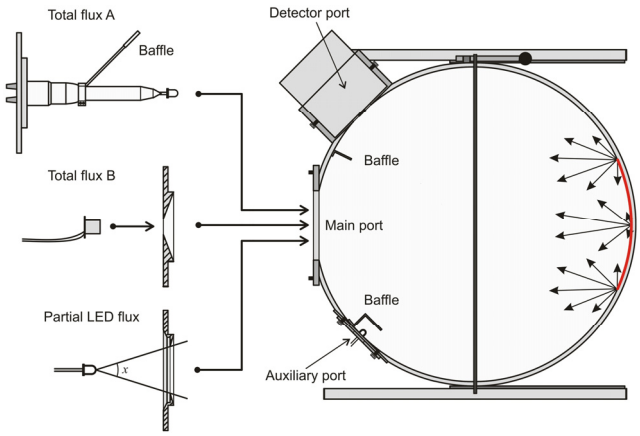

Figure 4. Multifunctional measurement setup for LED luminous flux [I].

Figure 5 shows the measurement setup configured for the calibration of the luminous flux responsivity with an external source, and for the three different luminous flux measurement geometries [8]. The responsivity calibration of the measurement setup is carried out by introducing a known external flux into the sphere through a 50-mm precision aperture. The same aperture is also used in the partial LED flux measurement. Due to the construction of the sphere, the light of the external source and the test LEDs illuminate the clear hemisphere in the same direction in all measurement geometries. As a result, the measurement uncertainty and the number of corrections needed are reduced. The responsivity of the partial flux mode can be transferred to the two total flux modes by measuring the signal level produced by the auxiliary source while changing the part in the main port. The auxiliary source is also used for the self-absorption measurement of the LED under calibration.

In the partial flux geometry, the LED is operated outside the sphere, and the light is collected through the 50-mm precision aperture. For total flux measurements of low-power LEDs in 4π geometry (Total flux A), a special LED-holder is used. The absorption of the backward emission of the LED has been minimized by using a thin holder with a reflective aluminum cone head [18]. The baffle needed in the measurement is an integral part of the holder. This ensures the correct placement of the baffle, and eliminates the need to touch the sensitive painted part when configuring the sphere for another measurement mode. The total flux of high-power LEDs in 2π geometry (Total flux B) can be measured by mounting the LED in a small

aperture. Large heatsinks can be used without affecting the responsivity of the sphere. The temperature of the LEDs can be adjusted in the range of 10 °C – 75 °C using a custom temperature controller, when measuring the partial flux or the total flux in the 2π geometry. When using the LED holder of the 4π geometry, the voltage of the LED is measured for monitoring its temperature.

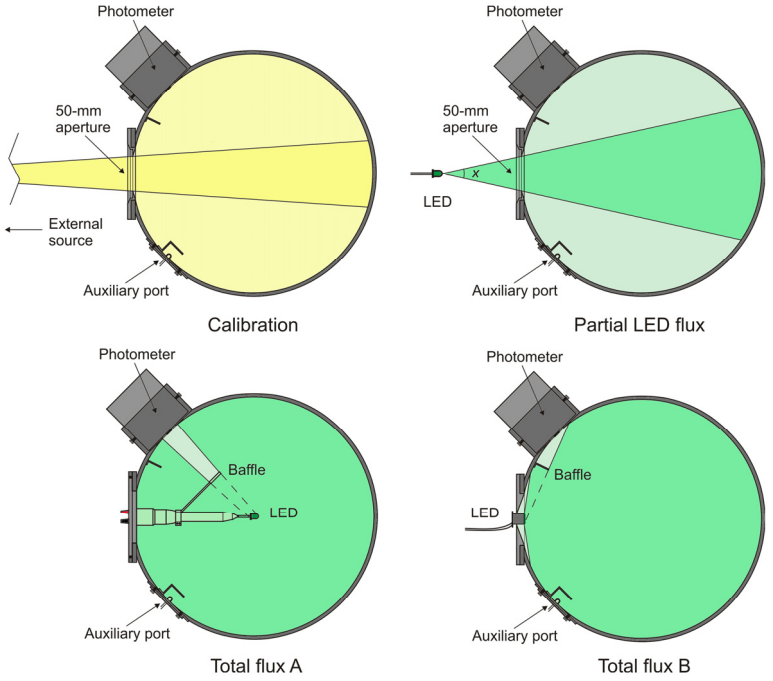

Figure 5. Illustration of the luminous flux responsivity calibration, and the three measurement geometries available with the sphere.

Measurement of the luminous flux of an LED consists of three consecutive measurements. First, the flux level produced by the LED is measured with the photometer. Then, the photometer is replaced with a spectroradiometer, and the spectral power distribution of the LED is measured. Finally, the self-absorption of the LED is measured using the photometer head and the auxiliary source (see Figure 6). In the self-absorption measurement, the flux level produced by the auxiliary source is compared between two cases, in which the test LED is attached in the sphere for measurement, and when it has been removed from the sphere [8]. The spectral mismatch correction is calculated using the measured LED spectrum, the relative spectral responsivity of the photometer head, and the spectral throughput of the sphere. The angular intensity distributions required for the spatial correction are determined using a compact goniometer [II].

Figure 6. Self-absorption measurement of a low-power LED configured for total flux measurement. All ports and baffles of the sphere are shown as well.

Due to the large variation in the optical properties of LEDs available [6-11], the measurement uncertainty is analyzed for each LED separately. The expanded uncertainty ($k = 2$) of the luminous flux measurement varies between 1.2 % and 4.6 %, depending on the measurement geometry, the spectrum and the angular spread of the test LED [I].

2.4 Spectral and spatial characterization of the sphere

Although a high quality photometer head with a spectral quality factor of $f_1' = 1.97 \pm 0.12$ % ($k = 2$) is used with the integrating sphere, a spectral mismatch correction is needed to reduce measurement uncertainties [III,8,16,37]. The relative spectral responsivity of the measurement setup was obtained by measuring separately the relative spectral responsivity of the photometer head [45] and the spectral throughput of the integrating sphere [40]. The measured relative spectral responsivities of the measurement setup, and the relative differences from $V(\lambda)$ in the 2π and 4π total flux measurement geometries are shown in Figure 7.

It can be seen that measurements of single-color LEDs require relatively large spectral mismatch corrections, a couple of percents. For white and green LEDs the corrections are smaller, typically less than 2 %. When measuring the spectra of white phosphor-coated LEDs, special care should be taken because the spectra of such LEDs often change depending on the angle of observation. For spectral mismatch correction, the spectra of the LEDs are measured using the integrating sphere in the same geometry as the luminous flux [I].

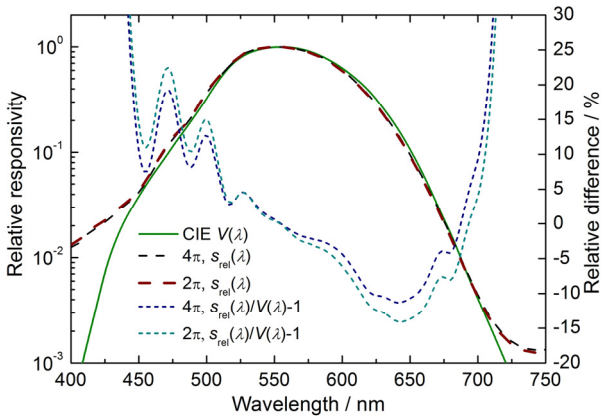

Figure 7. Relative spectral responsivities of the measurement setup, and the relative differences from $V(\lambda)$ in 2π and 4π measurement geometries.

Depending on the angular spread of the test LED, a spatial correction must be applied. The SRDF of the integrating sphere was scanned in horizontal and vertical directions using a rotary stage and a green collimated LED with a beam angle of ±1.5° [42]. Figure 8 shows an illustration of the spatial scanning of the sphere, and a luminous flux measurement of a batwing-LED that requires spatial correction. The results of the scanning showed that the variation in the spatial response is only ±1.5 % within the area, where the scanning beam does not illuminate the baffles directly [I].

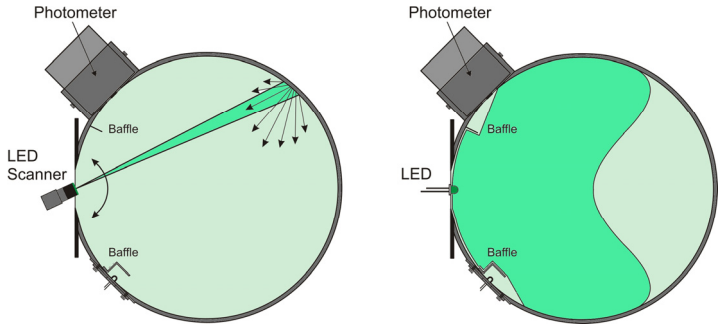

Figure 8. Spatial response scanning of the sphere (left) and luminous flux measurement of a batwing-LED (right).

For the analysis of the spatial correction factors, the effective SRDF of the sphere was calculated using the data of the vertical and horizontal scans, and by weighting them according to the geometry of the baffles. The spatial correction factor is obtained from the normalized spatial average of the SRDF weighted by the normalized angular intensity distribution of the LED. The behavior of the spatial correction factor was studied by modeling the angular intensity distributions of LEDs with different spreads [9]. The

analysis showed that the correction is less than 0.2 % for directional LEDs having a half width angle of ±40°. Higher corrections of the order of 0.5 – 2 % are needed only for special batwing- and side-emitting types of LEDs [I].

3. Luminous Efficacy Measurement of Solid-State Lamps

3.1 Solid-state lamps with E27-base

A typical retrofit E27-base SSL consists of LEDs, a built-in PSU, a heatsink, as well as some kind of optics covering the LEDs [14,25]. Figure 9 shows a selection of SSLs studied in [II]. Many SSL bulbs available have been designed to imitate the looks of a typical incandescent lamp. In addition, many lamps with unusual constructions are available. Some lamps do not have protection for the LEDs, whereas some may have the bulb filled with oil for thermal management. Most of the lamps are constructed using high-power LEDs. Due to the large variety of SSLs available in the market, selecting a good product may be problematic for an average consumer. Special care should be taken also in the characterization of the optical and electrical properties of SSLs. Due to the fact that SSLs contain LEDs, their optical properties can be complex [6-11,14].

Figure 9. A selection of E27-base SSLs studied in [II].

3.2 Measurement setup for luminous efficacy

In [II], a measurement setup was constructed for luminous efficacy measurements of SSLs using a 1.65-m integrating sphere, originally designed for measurements of incandescent standard lamps [40] (see Figure 10). SSLs use small built-in PSUs that convert the AC-voltage for the LEDs [29-32]. A programmable AC-power supply was acquired for operating the lamps. The electrical power consumption of the lamps is measured using a power meter. A separate current measuring amplifier is

used for analyzing the harmonic distortion of the power, and the quality of the lamp electronics.

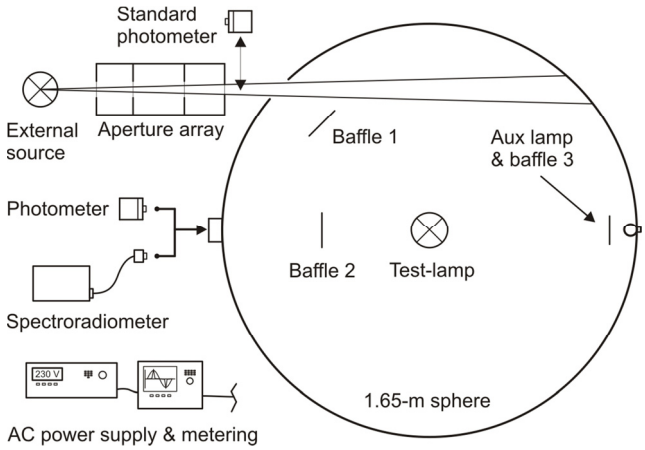

Figure 10. Luminous efficacy measurement setup of [II].

The original lamp holder of the sphere was replaced with a new slightly longer holder due to the smaller size of typical SSLs, as compared to typical luminous flux standard lamps. The longer holder ensures that the SSL is located at the center of the sphere, so that the baffles produce symmetrical shadows (see Figure 11). The wiring of the holder was also upgraded for the higher AC-voltage. The characterization measurements of the integrating sphere are conducted using the same methods, as for measurements of incandescent lamps [40]. However, the luminous flux responsivity is measured for an empty sphere, and the self-absorption of each SSL is measured [8,13,14,II].

Figure 11. Luminous efficacy measurement of an SSL. In addition to the holder, the detector port (left) and the reference port (right) are shown with their baffles.

The luminous efficacy measurement procedure is similar to the luminous flux measurement of LED-components [I]. First, the luminous flux and the electrical power of the SSL are measured. Then, the photometer is replaced with the spectroradiometer, and the relative spectral radiant flux is measured for the spectral mismatch correction, and for the average colorimetric quantities. Finally, the self-absorption of the SSL is measured.

3.3 Spectral self-absorption

During the luminous efficacy test measurements, it was found that the perceived spectrum of an SSL may change when it is operated inside an integrating sphere. In addition to the auxiliary lamp and the photometer, the self-absorptions of the lamps were measured using a scanning spectroradiometer. The spectral self-absorptions measured for 3 different SSLs are shown in Figure 12. Lamp no. 3 consists of blue LEDs and remote phosphor plates. We managed to measure the self-absorption of lamp 3 with (normal) and without the phosphor (modified). The difference between the two curves shows clearly the effect of the phosphor to the perceived spectrum. The errors caused by the spectral self-absorption in the value of luminous flux are negligible, if a relatively large integrating sphere is used. The errors are more evident when inspecting the colorimetric data. Corrections up to 17 K in the correlated color temperature (CCT) were obtained for the group of SSLs studied [II].

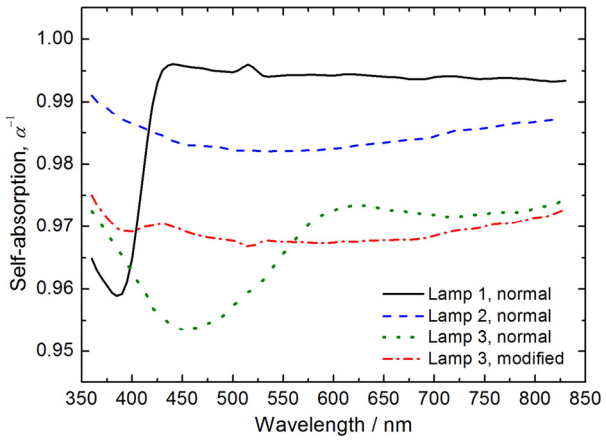

Figure 12. Spectral self-absorption of 3 different SSLs. Lamp no. 3 was also measured with the remote phosphor of the bulb removed (modified). [II]

3.4 Spatial correction

Although the LEDs of a typical bulb-type SSL are arranged to emit light into different directions, they are still somewhat directional, and a large part of the light is emitted towards the bottom of the sphere that is a common place for an integrating sphere to collect dust. In addition, the construction of the heatsink limits the backward radiation. This may not be a problem in the final application of the lamp, but needs to be considered in the luminous flux measurement due to the nonuniformity of the sphere reflectance [39-43]. The spatial correction factors are calculated for each SSL using its angular intensity distribution and the SRDF of the integrating sphere. The method is similar to that used in [I]. The SRDF of the 1.65-m integrating sphere, characterized using a sphere scanner [42] is presented in Figure 13.

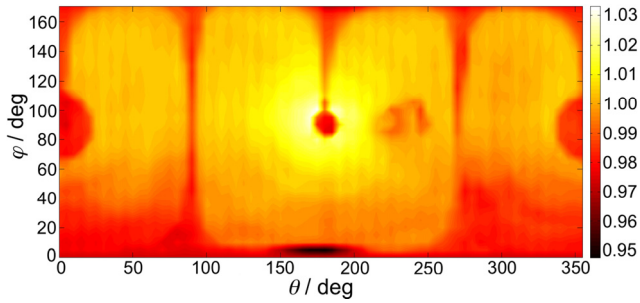

Figure 13. Spatial response distribution function (SRDF) of the 1.65-m integrating sphere, characterized using a sphere scanner.

For characterization of the angular intensity distributions of SSLs, a compact goniospectrometer was constructed [II]. It consists of two rotary stages for turning the lamp, a spectroradiometer with an array detector, and a cabinet for collecting the light. The distance from the SSL to the diffuser sheet collecting the light was selected to be the same as the radius of the integrating sphere. By doing so, the angular intensity distributions of SSLs are measured in a geometry close to that of the integrating sphere measurement. In addition to SSLs, the setup can be used for measurements of LED-components [I].

Figure 14 shows a luminous intensity distribution, and relative spectral irradiance measured as a function of the angle of observation for one of the SSL bulbs studied. The spatial correction factors obtained for typical bulb and spot types of lamps are between 1.001–1.007 and 1.009–1.013, respectively.

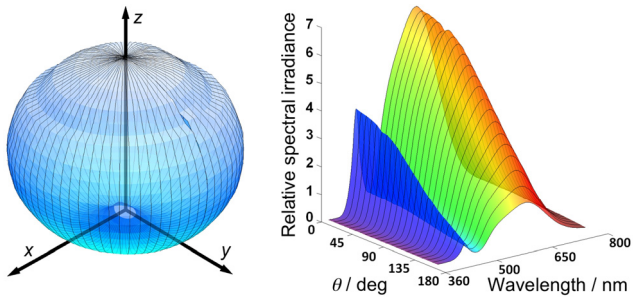

Figure 14. Luminous intensity distribution (left) and spectral irradiance as a function of angle of observation (right) measured for one of the studied SSLs.

In a typical goniophotometer designed for incandescent lamps, the lamp is rotated with the base pointing upwards to avoid permanent changes to the lamp characteristics [13,41]. In the case of SSLs, no damage is caused to the LEDs due to the change of the burning orientation. The only differences are due to the changes in the thermal operation of the lamp [6,25-28]. Comprehensive testing was carried out to find out the temperature differences of SSLs between the vertical and horizontal operating conditions. The differences in the temperature for the group of lamps tested were 0.1–2.5 °C. This causes only a negligible uncertainty in the spatial correction factor. The temperature variation of one of the SSLs during a 3-hour goniometer measurement is shown in Figure 15.

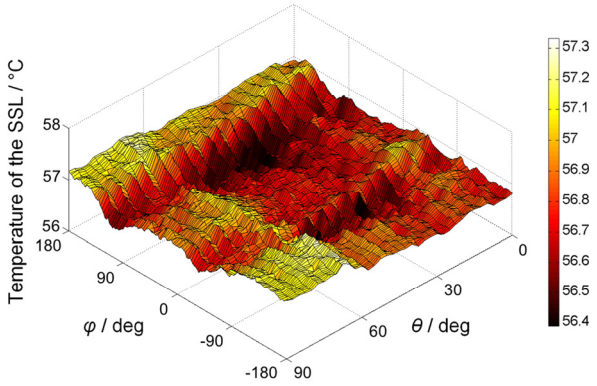

Figure 15. Temperature variation of an SSL during a 3-hour measurement with the goniospectrometer.

3.5 Luminous efficacy test measurements

The measurement setup was tested by measuring a group of 25 different SSLs available in the market. Large variations were found in the quality of the lamps, especially in the built-in PSUs. Some designs use just simple

rectifier bridges, whereas more expensive lamps may use switching power supplies with active control of the LEDs [29-32]. Most of the lamps tested produced pulsed luminous flux. The measured luminous efficacies for the group of lamps were between 25 lm/W and 64 lm/W, and the total harmonic distortions (THDs) were 30 – 280 %. Due to the high harmonic content of the power, the uncertainty of the electrical power measurement of SSLs is inevitably higher than that of DC-operated lamps.

Figure 16 shows the waveforms of the current, voltage and the luminous flux measured for one of the SSLs studied in [II]. For this lamp, the measured luminous efficacy is 53.9 lm/W and the deviation of the luminous flux from its mean value is ±31.4 %. The THD of the electrical current is 72 %. During the test-measurements, it was found that not all SSLs on the market can be measured with low uncertainty due to the possible instabilities caused by the built-in PSUs. The expanded uncertainty of the luminous efficacy measurement of a stable SSL is 1.2 % (k = 2).

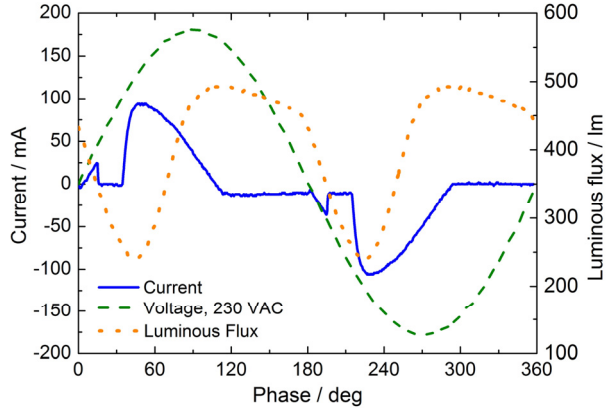

Figure 16. Waveforms of luminous flux and electrical power measurements for one of the SSLs studied in [II].

4. Photometer Spectral Quality Factor f_1'

4.1 Background and definition of f_1'

Photometers are designed to have spectral responsivity close to the CIE $V(\lambda)$-function that describes the luminous sensitivity of a human eye in photopic conditions [33]. In a typical illuminance measurement with a photometer, spectral mismatch error is caused due to the difference between the $V(\lambda)$ and the real spectral responsivity of the photometer. The mismatch can be corrected for, if the spectral responsivity of the photometer and the spectral power distributions of the light sources being measured are known [33]. This is important especially with single-color LEDs that require relatively large spectral corrections [I]. However, the spectral responsivities of photometers are often characterized for devices used in sophisticated measurement laboratories only, because the cost of such a calibration may not be reasonable for devices used in field measurements. For example with hand-held luxmeters, the user often needs to estimate the measurement uncertainty based on the specifications provided by the device manufacturer.

CIE quality factors are often used for reporting the performance of photometers in general lighting conditions. The quality factors are typically reported as percentage values. Although they cannot be used for applying corrections for measured values, they are important because a photometer with better characteristics typically leads to lower measurement uncertainties due to smaller correction factors needed. One of the CIE quality factors is the spectral quality factor f_1' [33]. It gives information on the possible errors introduced when measuring broadband light sources without spectral mismatch correction. The quality factor f_1' is defined by equation

$$f_1' = \frac{\int \left| s^*_{\mathrm{rel}}(\lambda) - V(\lambda) \right| \mathrm{d}\lambda}{\int V(\lambda)\,\mathrm{d}\lambda}, \qquad (1)$$

where $s^*_{\mathrm{rel}}(\lambda)$ is the normalized relative spectral responsivity of the photometer, that is

$$s^*_{\mathrm{rel}}(\lambda) = s_{\mathrm{rel}}(\lambda) \cdot \frac{\int S_{\mathrm{A}}(\lambda) \cdot V(\lambda)\,\mathrm{d}\lambda}{\int S_{\mathrm{A}}(\lambda) \cdot s_{\mathrm{rel}}(\lambda)\,\mathrm{d}\lambda}, \qquad (2)$$

where $S_A(\lambda)$ is the relative spectral distribution of the CIE standard illuminant A and $s_{rel}(\lambda)$ is the relative spectral responsivity of the photometer. Ideally, if $s^*_{rel}(\lambda) = V(\lambda)$, then $f_1' = 0$ %. Although the CIE quality factors have been used by the photometer manufacturers and the lighting industry for years, no official methods for determining the uncertainties of the quality factors have been published. This makes selection of such a device problematic. A question arises whether the customer can trust the specifications reported for a device or not?

4.2 Characterization of the relative spectral responsivity

The spectral responsivity of a photometer head is typically characterized using a spectrally tunable light source. For this purpose, either a tunable laser or a broadband light source with a monochromator is used [37, 45-47]. In the measurement, the current produced by the photometer at each wavelength is compared to the signal of a reference detector with known spectral responsivity.

In order to study the uncertainty of the quality factor f_1', the relative spectral responsivities of two photometer heads (see Figure 17) were characterized using a reference spectrometer [45]. The setup consists of an incandescent light source, a monochromator, and a linear translator for moving the photometer and the reference trap detector. The characterization of the photometers was conducted within the photometric wavelength range of 360–830 nm with a step of 1 nm.

Figure 17. A photograph of the two photometer heads studied in [III].

The normalized relative spectral responsivity of one of the photometers measured in [III], and the difference curve $s^*_{rel}(\lambda)$-$V(\lambda)$ with the expanded uncertainty are shown in Figure 18. Due to the relatively good

spectral matching of the two photometers, the effect of the normalization of equation 2 is less than 0.01 % to the level of the responsivities, as compared to the responsivities normalized to unity at 555 nm [III].

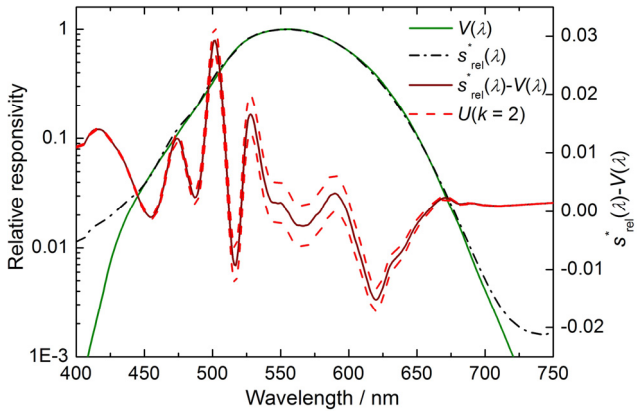

Figure 18. Normalized relative spectral responsivity of one of the photometers studied in [III] and the difference from the $V(\lambda)$-function.

4.3 Random and biased error models

For evaluation of the uncertainty of the f_1', the spectral responsivity of the photometer and the uncertainty budget of the characterization measurement are needed. Due to the definition of f_1', its uncertainty evaluation using analytical methods is difficult [34]. The uncertainty of f_1' is often evaluated using Monte Carlo simulation. In the analysis, a large number of f_1' values are calculated using spectral responsivities, which have been perturbed within the measurement uncertainties. As a result, a distribution of f_1' values is obtained giving the uncertainty of the quality factor [35-38].

Monte Carlo simulation is often carried out by randomly varying the individual data points of the spectral responsivity data [35,36]. The principle of the method is illustrated in Figure 19. When using this model, the data is perturbed within the uncertainties by weighting the uncertainty of each wavelength by a separate random number. The method assumes no correlation between the wavelengths, and can be used for type A uncertainties, for example measurement noise. However, the spectral responsivity measurement of a photometer typically has biased uncertainties of type B, which cannot be simulated by randomly perturbing the values. For analyzing the effects of type B uncertainties, more sophisticated error models need to be derived for the characterization measurement [III].

Measurement of the spectral responsivity with a monochromator-based setup may have a large biased contribution due to the wavelength scale uncertainty. This is also the case with the measurement setup used for the measurements of [III]. The wavelength setting uncertainty of the monochromator is ±0.06 nm. In order to simulate the effect of this biased uncertainty, an error function was derived using the derivatives of the spectral responsivities of the photometer and the reference detector. As a result, a curve was obtained that changes its polarity at 555 nm, the peak of the spectral responsivity. The biased error model is shown in Figure 20. In the simulation, the curve of the biased wavelength uncertainty is multiplied by a single random number that defines the magnitude and the polarity of the uncertainty. A set of oscillating functions is obtained that effectively shift the spectral responsivity towards higher or lower wavelengths, simulating the true behavior of the uncertainty.

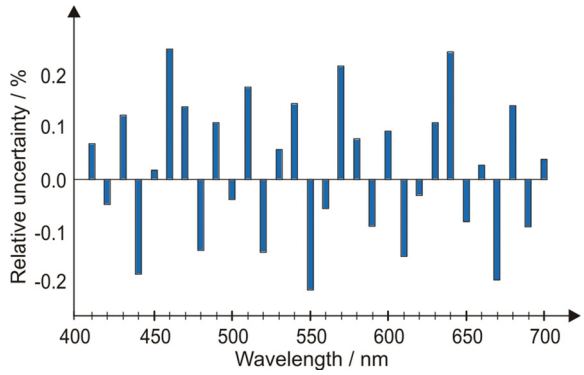

Figure 19. Monte Carlo simulation with random error model. No correlation is assumed between neighboring data points.

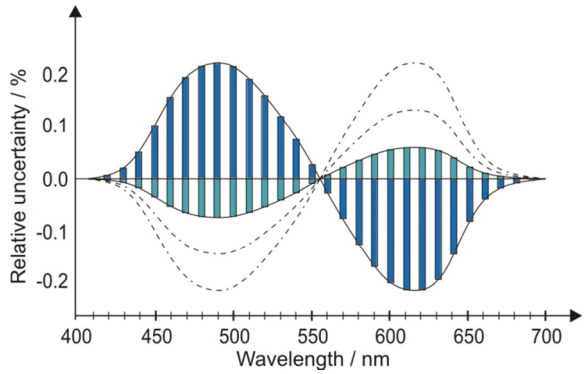

Figure 20. Monte Carlo simulation with biased error model. Neighboring wavelengths have strong correlation.

4.4 Simulation results

The uncertainty simulations were conducted using 100 000 repetitions and 400 wavelength steps in the range of 380–780 nm. Typical results of the simulation are shown in Figure 21. The biased distribution was obtained using the developed biased error model and the wavelength uncertainty of the measurement, whereas the random distribution was achieved by testing a case where all uncertainties of the measurement were treated as random uncertainties. It is clearly shown that the random error model produces much smaller uncertainty of f_1', for this photometer, only 20 % of the uncertainty obtained using the biased error model.

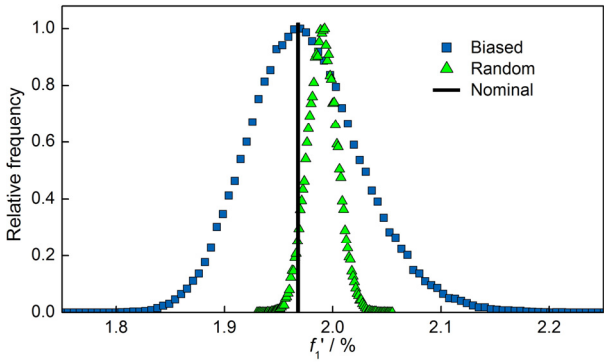

Figure 21. Simulated f_1' distributions for one of the photometers studied, obtained with the biased and random error models [III].

Due to the definition of f_1', any deviation of the photometer spectral responsivity from the $V(\lambda)$ causes an increased value of f_1', indicating that the measurement uncertainty may influence the value of the f_1' itself. This can be seen in the distribution obtained with the random error model. Similar effect was found also in [36]. The mean value of the distribution (f_1' = 1.99 %) is higher than the nominal value (f_1' = 1.97 %), shown as a single vertical line in Figure 21, calculated with zero uncertainty [III]. In addition, the wavelength step used in the analysis affects the uncertainty of f_1'. By decreasing the number of wavelength steps, higher uncertainty of f_1' is obtained.

The simulation results demonstrate that the uncertainty of f_1' can change quite dramatically, depending on how the uncertainties are treated in the simulation. The biased error model gives more realistic estimates for the wavelength uncertainty than the random error model. When both error models are combined in the analysis, it can be seen that the biased uncertainties dominate the total uncertainty of f_1'. The methods developed in [III] can be extended by including biased error functions of higher

degrees in the analysis [38]. The developed methods are also applicable for calculating the uncertainties of other quality factors and integral quantities.

5. Photometer Directional Response Index f_2

5.1 Definition of the quality index f_2

Illuminance meters are typically equipped with diffusers for obtaining cosinusoidal directional response. Quality index f_2 quantifies the quality of the matching of the directional response with the cosine function [33]. The directional response of a photometer is characterized by measuring a small light source located far away, and rotating the photometer to change the direction of the light incident on the receiving plane of the photometer. The directional response of the photometer to the incident radiation is characterized by

$$f_2(\varepsilon,\varphi) = \frac{R(\varepsilon,\varphi)}{R(0,\varphi)\cos\varepsilon} - 1\,, \tag{3}$$

where $R(\varepsilon,\varphi)$ is the signal output of the photometer as a function of the angle of incidence ε, and the azimuth angle φ. The angle ε is measured with respect to the normal of the acceptance area of the photometer. The angle φ is the rotation angle of the photometer around its optical axis. The directional response is measured in at least two mutually perpendicular planes. These planes correspond to the azimuth angles of φ = 0, π/2, π, and 3π/2. The quality index f_2 of each azimuth angle is calculated using

$$f_2 = \int_0^{1.484} \left| f_2(\varepsilon,\varphi) \right| \cdot \sin 2\varepsilon \, \mathrm{d}\,\varepsilon\,, \tag{4}$$

where the upper limit of the integral corresponds to 85° in degrees.

5.2 Characterization of the directional response

In [IV], the photometric directional responses of three photometers were measured for studying the uncertainty of f_2 using Monte Carlo simulation. The front planes of the photometers studied are shown in Figure 22. All photometers had flat circular diffusers. The diameters of the diffusers were 7 mm, 16 mm and 32 mm for photometers 1, 2 and 3, respectively. Photometers 1 and 2 were equipped with shadow rings around their diffusers.

The directional response measurements were conducted using a stable incandescent light source, a servo-controlled rotary stage and a photometric bench with baffles for straylight rejection. The distance between the light source and the photometer under measurement was

d = 2.5 m. The directional response of each photometer was measured in a total of four planes, resulting in 8 values of f_2. All measurements were conducted within an angular range of $-90° \leq \varepsilon \leq 90°$ with a step of 1°. In order to study the sensitivity of the photometer alignment to the value of f_2, several additional measurements were conducted for each photometer by intentionally misaligning the photometer from its initial position.

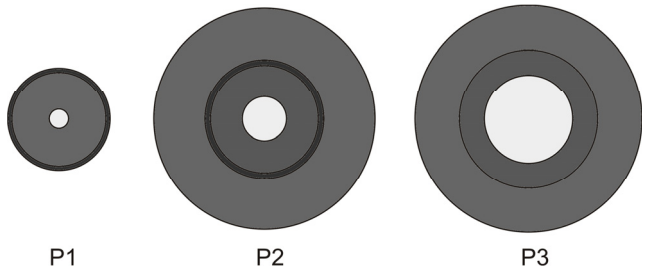

Figure 22. Front planes of the three photometers studied in [IV].

5.3 Overview of the error models

For analyzing the uncertainty of f_2, the methods developed for the uncertainty analysis of f_1' [III] were used as the basis for deriving a total of five error models for the simulations. A simulation program was constructed that runs both random and biased errors simultaneously, taking into account the measurement noise, drift of the light source, alignment of the photometer, and the errors of the rotary stage. Table 1 lists the characteristics of the uncertainty components of the directional response measurement, as well as the number of the error model, which is used for simulating the contribution of the particular uncertainty.

Table 1. Uncertainty components of the directional response measurement.

Component	Uncertainty	Unit	Distribution	Type	Model
Photometer					
Noise	0.005	%	Gaussian	Random	1
Light source					
Drift	0.05	%	Rectangular	Biased	2
Alignment					
z-axis (longitudinal)	0.5	mm	Rectangular	Biased	3
x-axis (transverse)	0.5	mm	Rectangular	Biased	3
y-axis (angle ε)	0.05	deg	Rectangular	Biased	4
Azimuth angle φ	1	deg	Rectangular	Biased	5
Rotary stage					
Accuracy	80	arcsec	Rectangular	Biased	4
Repeatability	3	arcsec	Rectangular	Biased	4
Resolution	6.5	arcsec	Rectangular	Random	4

In the simulation, two mutually perpendicular directional responses are first perturbed with the error models, after which the distributions of f_2

are calculated using equations 3 and 4. The process is repeated 100 000 times. The measurement noise and the resolution of the rotary stage are treated as random uncertainties. All other uncertainties are treated as biased uncertainties. Error model 1 adds noise to the measured response based on the average noise of the measurement. Error model 2 models the drift of the light source on the basis of the readings of the monitor detector used in the measurements.

Error model 3 models the geometrical alignment error of the photometer in the transverse and longitudinal directions with respect to the optical axis of the measurement. The model calculates the relative error in the measured illuminance that is caused by the asymmetric rotation of the photometer head around the center of the rotary stage. If the photometer is misaligned, the effective distance from the receiving plane of the photometer to the light source changes as a function of the angle of rotation. In addition, the alignment error causes an error in the effective angle of rotation, which is taken into account by error model 4 that calculates the errors of the rotary stage. Figure 23 shows a group of error curves calculated using error model 3 with random input parameters for the alignment with measurement distance of d = 2.5 m. The errors printed with the same colors and numbering have been calculated using the same error parameters.

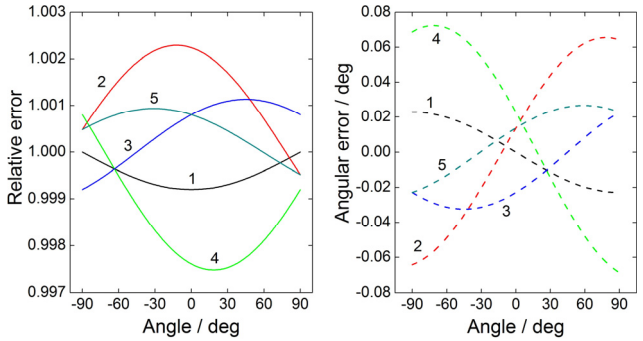

Figure 23. Relative error of the measured illuminance (left) and absolute error of the angle of rotation (right) of error model 3.

Error model 4 takes into account the uncertainty of setting the zero angle of the photometer using a two-beam alignment laser, and the errors of the rotary stage. The basis of error model 4 is the derivative of the measured directional response, which gives the sensitivity of the error. The accuracy and repeatability of the rotary stage are treated as biased uncertainties, whereas the resolution of the stage is treated as a random

uncertainty. The angular error parameter of error model 3 is used as one of the input parameters of error model 4 as well.

CIE Publication 69 [33] does not give recommendations about how the zero azimuth of the two perpendicular planes of the photometer should be selected for the directional response measurement. In a typical illuminance measurement, the alignment of the azimuth angle is not critical. However, the results of [IV] showed that the directional responses of a photometer measured in two perpendicular planes may differ from each other. Error model 5 models the error in the alignment of the azimuth angle of the photometer. The model assumes that the response of the photometer changes between the responses measured in the two perpendicular planes. The error is calculated as a linear combination of the two responses. For the three photometers, the linear combination of the responses measured in two perpendicular planes, in most cases, gives a response close to the one measured using an azimuth angle between the two planes. Due to the asymmetry of the responses, the method is not perfect, but gives a reasonable estimate of the error for the purpose of the uncertainty analysis.

Figure 24 shows a random selection of perturbation curves calculated with the error model 4 and combined errors for a photometer with a perfectly cosinusoidal directional response. The biased shapes of error model 4 are based on the derivative of the directional response. The noise of the model originates from the resolution of the rotary stage. The curves of the combined errors show the effect of all error models working in combination. It can be seen that the biased errors of the measurement have much larger contribution to the uncertainty of the directional response than the random error components. The various shapes of the combined errors are a result of the complexity of the simulation.

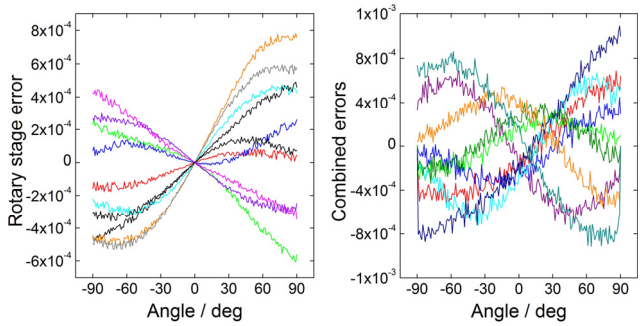

Figure 24. Random selection of perturbation curves of error model 4 (left) and combined errors of all models (right) for a perfectly cosinusoidal photometer.

5.4 Simulation results

Figure 25 shows the simulated f_2 distributions for photometer P1, studied in [IV] and for a photometer with a perfectly cosinusoidal response, denoted as P_{cos}. The blue (h) and green (v) distributions were obtained from the responses measured in the horizontal and vertical planes, respectively. The dark grey distributions represent the f_2 calculated as an average of the f_2 values of each azimuth. The nominal values of f_2, calculated without uncertainties are shown with black vertical bars.

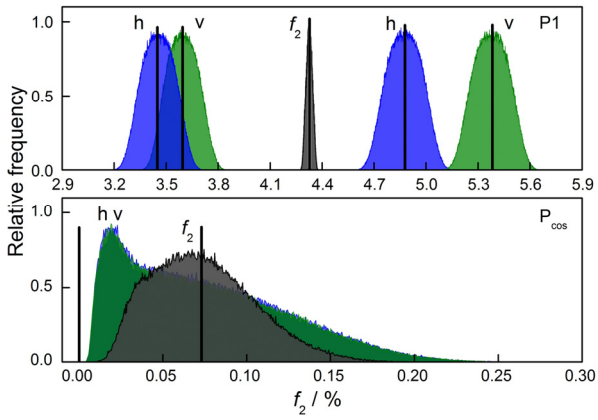

Figure 25. Simulated f_2 distributions for photometer P1 of [IV], and for photometer P_{cos} with a perfectly cosinusoidal response. For colors and symbols, see text.

The results show that the values of the quality index f_2 of each azimuth angle of a photometer can be highly sensitive to the asymmetry of the measured directional response. The responses of photometers P1 and P2 were more asymmetric than the response of photometer P3. It is possible that the asymmetric response is caused by the manufacturing tolerances of the photometer, for example the alignment of the diffuser with respect to the mechanical symmetry axis. This hypothesis is supported by the fact that photometers P1 and P2 were aligned by placing an alignment mirror against their aluminum shadow rings, whereas photometer P3 was aligned using its large diffuser surface as the base for the mirror. It was further demonstrated by modifying the symmetry of the measured responses that the average f_2 is relatively insensitive to the asymmetry of the photometer directional response, and can be used more reliably for determining the value of the quality index f_2 than the individual f_2 values of each azimuth.

The f_2 of photometer P1 analyzed as the average of all simulated values was 4.325 ± 0.035 % (k = 2). All three photometers were remeasured

by selecting different azimuth angles for the measurements. The results agree with each other within the simulated uncertainties. The nominal values of f_2 do not necessarily coincide with the mean values of the distributions either. Similar behavior was found earlier with the spectral quality factor f_1' [36, III]. The majority of the simulations was run using a step of 5°. By using a step of 1°, the average f_2 values obtained were smaller by approximately 5 times the simulated uncertainties, while the changes in the uncertainties were small. The results suggest that the step of 5° may be too large for the analyzing the quality factor f_2, and the step of 1° should be used instead.

The simulation program was tested also with a perfectly cosinusoidal directional response, using the same uncertainties as for the three real photometers (see Figure 25). The average f_2 obtained for the perfectly cosinusoidal photometer P_{cos} was 0.074 ± 0.062 % (k = 2). The value cannot reach 0 % due to the uncertainties and the absolute value-brackets of the definition of f_2. The f_2 distributions of each azimuth angle of photometer P_{cos} have a peak close to the smallest simulated values. The distribution of the average f_2 differs from the others because there is no correlation between the measurements conducted in the two perpendicular planes. Each photometer was realigned when changing the azimuth angle of the measurement. In the simulation, this has been taken into account so that both responses of a photometer are treated with their own sets of random numbers.

5.5 Position of the rotational axis

The functionality of the error models of [IV] was verified by several additional measurements, in which the photometer was intentionally misaligned from its initial position. The simulated f_2 values of the three photometers agree with the values measured with deviations up to ±2 mm from the initial position. The simulation program allows to test how the measured directional response would change if the photometer had diffuser offset d_0 [48-51], and if it was aligned for the measurement according to that plane instead of the front surface of the diffuser. In the measurements, this can be obtained by adjusting the position of the axis of rotation by moving the photometer in the longitudinal direction on the rotary stage.

In addition to the tests conducted with alignment errors up to ±2 mm, the effect of the diffuser offset d_0 to the value of f_2 was simulated in a much wider range of -150 mm ≤ d_0 ≤ 150 mm. The f_2 values obtained for

the three photometers with d_0 = 0 mm were 4.325 %, 1.698 % and 4.315 %. By using diffuser offset values of 41.6 mm, -18.6 mm and -59.4 mm in the simulation, significantly better f_2 values of 1.423 %, 1.037 % and 1.224 %, respectively, were obtained for the same photometers. Positive diffuser offset values here mean that the receiving plane of the photometer is located inside the photometer. The results of the simulations suggest that for any photometer, it is possible to find a virtual minimum value of f_2 by selecting the position of the axis of rotation with respect to the receiving plane of the photometer differently in the directional response measurement. The effect is heavily dependent on the measurement distance. It can compensate for the deviations between the photometer response and the cosine function, if a typical measurement distance of a couple of meters is used. Tests with the perfectly cosinusoidal photometer data showed that the value of f_2 only increases, if the diffuser offset value is changed, as can be expected. If the simulation is run with an infinite distance between the source and the photometer, the effect disappears.

5.6 Measurements with large diffuser offset values

The functionality of the simulation program with very large diffuser offset values was later verified by measuring the directional responses of two photometers using offset values up to $|d_0|$ = 110 mm. Because the three photometers studied in [IV] were not available for these tests, the measurements were conducted for two different photometers. The initial measurements were conducted in the horizontal plane at a distance of d = 2.66 m from the light source. The normalized directional responses $R(\varepsilon,0)/R(0,0)$ of photometers P4 and P5, and their difference curves $[R(\varepsilon,0)/R(0,0)]$-cos($\varepsilon$) are shown in Figure 26.

Photometer P4 is typically used in measurements of LEDs and SSLs with integrating spheres [I,II]. It has a flat diffuser with a diameter of 8 mm, and a shadow ring around the diffuser. The characterized directional response of photometer P4 showed that it is a high quality instrument with f_2 = 0.799 ± 0.022 %. Photometer P5 has a flat diffuser mounted in a recess behind an aperture with a diameter of 11.3 mm. Due to the construction, the signal values drop rapidly towards large angles of ε. The characterized directional response of photometer P5 revealed poor quality with f_2 = 12.833 ± 0.024 %. This photometer is not used with integrating spheres, but has been designed for measurement of the averaged LED intensity according to [8].

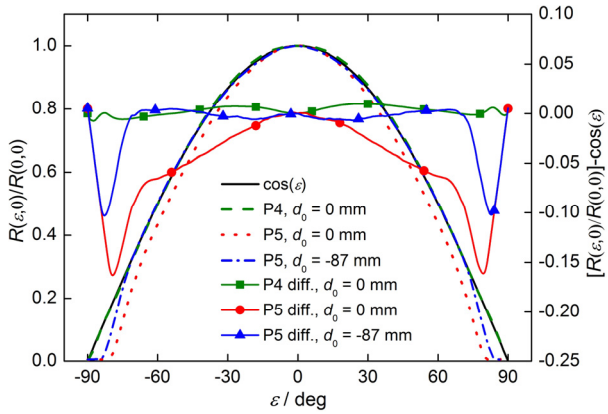

Figure 26. Characterized directional responses $R(\varepsilon,0)/R(0,0)$ of photometers P4 and P5, and their difference curves $[R(\varepsilon,0)/R(0,0)]$-cos($\varepsilon$). Photometer P5 was measured also with d_0 = -87 mm to obtain the virtual minimum value of f_2.

After the initial measurements with d_0 = 0 mm, the simulation was run to find the virtual minimum values of f_2 for the photometers. The minimum f_2 values of photometers P4 and P5 could be found using d_0 = 3 mm and d_0 = -150 mm, respectively. Due to the fact that the adjustment of d_0 was mechanically limited to ±110 mm, the virtual minimum value of f_2 could not be measured for photometer P5 at a distance of d = 2.66 m from the source. If a distance of d = 1.50 m was used instead, the virtual minimum value of f_2 could be found using a smaller diffuser offset value of d_0 = -87 mm, which was still within the mechanical limits of the setup. The simulated and measured f_2 values of the two photometers as a function of d_0 are presented in Figure 27. The simulated values of photometers P4 and P5 are drawn with black solid curves. The measured values are marked using green squares and red circles, respectively.

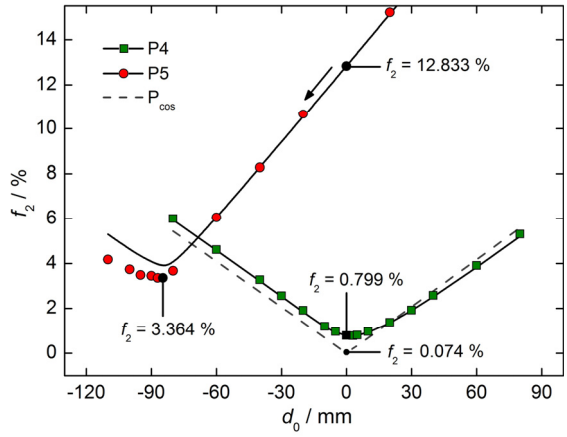

Figure 27. Measured and simulated f_2 values of photometers P4 and P5 as a function of the diffuser offset d_0. For colors and symbols, see text.

The f_2 values measured for photometer P4 at a distance of d = 2.66 m follow closely the simulated curve in the whole offset range of -80 mm < d_o < 80 mm. The largest deviation between the measured and simulated f_2 values is 0.104 %-units at d_o = 80 mm. The virtual minimum value of f_2 for photometer P4 was found in the measurements at d_o = 3 mm, as suggested by the simulations, resulting in f_2 = 0.787 ± 0.022 %, which is 0.012 %-units smaller than the f_2 measured with d_o = 0 mm. In practice, due to the high quality matching of photometer P4, the f_2 only increases by changing the offset value, as is the case with the perfectly cosinusoidal directional response P_{cos}, presented with black dashed line in Figure 27.

Due to the fact that changing the diffuser offset value in the measurements effectively expands or compresses the directional response, the response of photometer P5 could be improved by conducting the measurement with offset values of d_o < 0 mm. As suggested by the simulation, the virtual minimum value of f_2 for photometer P5 was found at d_o = -87 mm (see Figure 27), resulting in f_2 = 3.364 %. The value is 9.469 %-units smaller than the nominal f_2 value of the photometer. In the measurement, the photometer head rotated 87 mm behind the axis of rotation and recorded less signal at ε = 0° compared to the larger angles of ε, producing a much better match with the cosine function, as demonstrated in Figure 26. The deviations between the measured and simulated values are less than 0.145 %-units within the range of -60 mm < d_o < 60 mm. With d_o < -60 mm, the measured values deviate up to 1 %-unit from the simulated values. This is likely caused by the unusually large offsets used in the measurements (see Figure 28), the straylight due to the interreflections between the photometer and the baffles, as well as the nonisotropic behavior of the lamp at the shorter measurement distance.

The test measurements showed that the functionality of the error models is very good even with unusually large diffuser offset values or alignment errors, if a measurement distance of at least 2.5 m is used in the measurements, and the straylight can be avoided. The tests also prove that it is possible to find a virtual minimum value of f_2 for a photometer by changing the position of the axis of rotation in the measurement. However, it must be emphasized that although the results are interesting, using such a high diffuser offset values for a photometer most probably would not obey the inverse square law, and should not be used for determining the f_2 of a photometer. Earlier studies show that offsets of flat diffusers are close to 0 mm, and less than 10 mm for typical dome-shaped diffusers [48,50].

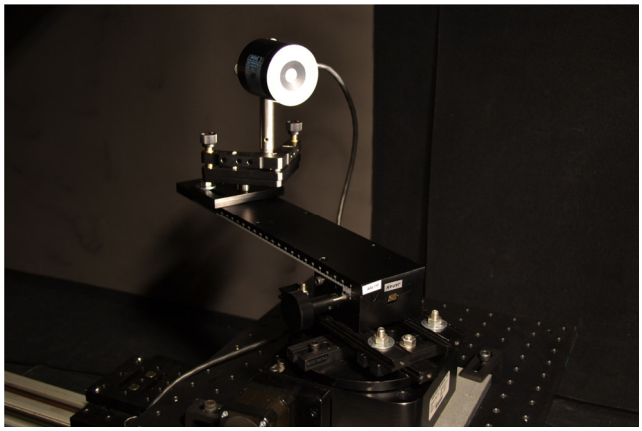

Figure 28. Directional response measurement of photometer P5 with diffuser offset d_0 = -110 mm.

Although CIE Publication 69 [33] recommends that the position of the axis of rotation in the directional response measurement should coincide with the center of the acceptance area of the photometer, it still gives the manufacturers a freedom to describe any other point for this axis. This issue should be addressed in any future version of the CIE Publication, so that the values of f_2 measured by different manufacturers could be reliably compared with each other.

6. Conclusions

In this thesis, measurement setups have been constructed and characterized for luminous flux and luminous efficacy measurement of LEDs and SSLs. The spectral responsivities and directional responses of photometers needed in the measurements have been characterized. Methods have been developed for analyzing the uncertainties of the photometer spectral and directional quality indices f_1' and f_2 using Monte Carlo simulation with error models derived for the characterization measurements.

A custom-made 30-cm integrating sphere has been characterized for the total and partial luminous flux measurements of low- and high-power LEDs. All measurement geometries of the CIE Publication 127 can be realized with the setup. The design of the sphere has been optimized for spatial uniformity by minimizing the amount and the area of the ports and baffles. The beams of the calibration source and the LEDs under calibration illuminate the sphere in the same direction in all measurement geometries. Spatial correction factors smaller than 0.2 % are obtained for typical directional LEDs. The expanded uncertainty ($k = 2$) of the luminous flux measurement varies between 1.2 % and 4.6 %, depending on the color and the angular spread of the LED.

A setup based on a 1.65-m integrating sphere and a compact goniospectrometer has been developed for luminous efficacy measurements of SSLs. Results of test-measurements conducted for a group of 25 different E27-base SSLs show large differences in the luminous efficacies, and in the quality of the built-in power supplies. The measured luminous efficacies for the group of lamps tested are between 25 lm/W and 64 lm/W, and the total harmonic distortions of the electrical currents are 30 – 280 %. Most of the lamps produce pulsed luminous flux. It has been found that self-absorptions of SSLs have spectral dependence, and change the perceived spectral radiant flux inside an integrating sphere. The resulting corrections for luminous flux are small, but the effect needs to be taken into account with colorimetric quantities. The luminous efficacy of a typical SSL with stable electronics can be measured with 1.2 % ($k = 2$) expanded uncertainty.

The applicability of biased and random error models for determining the uncertainty of photometer spectral quality factor f_1' has

been studied using Monte Carlo simulation with spectral responsivities measured of two photometers. The simulation results show that the random error model alone may easily underestimate the uncertainty of f_1'. The real effect of the biased uncertainty components, such as the wavelength scale uncertainty of a monochromator, on the uncertainty of f_1' can only be evaluated with more sophisticated models, such as the biased error model. By combining the random and biased error models in the simulation, it can be seen that the biased uncertainties dominate the total uncertainty of f_1'.

The directional responses of three photometer heads have been characterized for analyzing the uncertainties of photometer quality index f_2. In the analysis, Monte Carlo simulation is used with random and biased error models, derived for the characterization measurement. The values of f_2 obtained for each azimuth angle of a photometer are highly sensitive to the asymmetry of the photometer construction. Further tests show that the f_2 calculated as an average of all simulated values is relatively insensitive to the asymmetry, and can be more reliably used for determining the value of f_2 than the individual f_2 values of each azimuth. It has also been found that with typical measurement distances, the position of the axis of rotation with respect to the receiving plane of the photometer affects the value of f_2.

The methods developed for the uncertainty analysis of the photometer quality indices f_1' and f_2 give a solid basis for the uncertainty analysis of other quality indices and integral quantities used in photometry.

References

[1] S. Nakamura, T. Mukai, and M. Senoh, "Candela-class high-brightness InGaN/AlGaN double-heterostructure blue-light-emitting diodes," *Appl. Phys. Lett.* **64**, 1687–1689 (1994).

[2] D.A. Steigerwald, J.C. Bhat, D. Collins, R.M. Fletcher, M. Ochiai Holcomb, M.J. Ludowise, P.S. Martin, and S.L. Rudaz, "Illumination with solid state lighting technology," *IEEE J. Sel. Top. Quantum Electron.* **8**, 310–320 (2002).

[3] J.K. Sheu, S.J. Chang, C.H. Kuo, Y.K. Su, L.W. Wu, Y.C. Lin, W.C Lai, J.M. Tsai, G.C. Chi, and R.K. Wu, "White-light emission from near UV InGaN-GaN LED chip precoated with blue/green/red phosphors," *IEEE Photon. Technol. Lett.* **15**, 18–20 (2003).

[4] N. Narendran, Y. Gu, J.P. Freyssinier-Nova, and Y. Zhu, "Extracting phosphor-scattered photons to improve white LED efficiency," *Phys. Stat. Sol.* **202**, R60–R62 (2005).

[5] E.F. Schubert and J.K. Kim, "Solid-state light sources gettings smart," *Science* **308**, 1274–1278 (2005).

[6] S. Chhajed, Y. Xi, Y.-L. Li, Th. Gessmann, and E.F. Schubert, "Influence of junction temperature on chromaticity and color-rendering properties of trichromatic white-light sources based on light-emitting diodes," *J. Appl. Phys.* **97**, 054506 (2005).

[7] G.T. Gillies, "Altered light-emitting diode point source emitter," *Am. J. Phys.* **48**, 418–419 (1980).

[8] CIE 127-2007, *Measurement of LEDs*, 2nd ed. (Commission Internationale de l'Eclairage, Vienna, Austria, 2007).

[9] P. Manninen, J. Hovila, P. Kärhä, and E. Ikonen, "Method for analysing luminous intensity of light-emitting diodes," *Meas. Sci. Technol.* **18**, 223–229 (2007).

[10] I. Moreno and C.C. Sun, "Modeling the radiation pattern of LEDs," *Opt. Express* **16**, 1808–1819 (2008).

[11] M Bürmen, F. Pernus, and B. Likar, "LED light soures: a survey of quality-affecting factors and methods for their assessment," *Meas. Sci. Technol.* **19**, 122002 (2008).

[12] International Lighting Vocabulary CIE Publ. No 17.4/ IEC Publ. 50 (International Commission on Illumination / International Electrotechnical Commission, 1987/1989).

[13] The Measurement of Luminous Flux CIE Publ. No 84 (Vienna: International Commission on Illumination, 1989).

[14] IES LM-79-08 Approved Method: Electrical and Photometric Measurements of Solid-State Lighting Products (New York: Illuminating Engineering Society, 2008).

[15] C. C. Miller and Y. Ohno, "Luminous Flux Calibration of LEDs at NIST," Proc. 2nd CIE Expert Symposium on LED Measurement, Gaithersburg, MD, 45 (2001).

[16] K. Godo, T. Saito, H. Shitomi, T. Zama, and I. Saito, “Development of a total luminous flux measurement facility for LEDs at the National Metrology Institute of Japan,” Proc. NEWRAD 2005, 199 (2005).

[17] S. Park, Y.W. Kim, D.H. Lee, and S.N. Park, “Preparation of a standard light-emitting diode (LED) for photometric measurements by functional seasoning,” *Metrologia* **43**, 299–305 (2006).

[18] M. Lindemann, R. Maass, M. Taddeo, R. Mehrotra, and A. Sperling, “Reliable Photometric and Radiometric Measurements of bare LEDs and High Power LEDs using special LED Holder,” Proc. NEWRAD 2008, 227 (2008).

[19] S. Park, D. H. Lee, Y. W. Kim, and S. N. Park, “Absolute Integrating Sphere Method for Total Luminous Flux of LEDs,” Proc. NEWRAD 2008, 215 (2008).

[20] G. Brida, M. L. Rastello, F. Saccomandi, and F. Viarengo, “A combined method for measuring total flux and luminous intensity of LEDs,” Proc. CIE Expert Symposium on Advances in Photometry and Colorimetry, Turin, Italy, 107 (2008).

[21] K. Oshima, K. Ohkubo, and S. Mishima, “The new idea for total luminous flux measurement,” Proc. CIE Expert Symposium on Advances in Photometry and Colorimetry, Turin, Italy, 128 (2008).

[22] M. Lindemann and R. Maass, “Photometry and colorimetry of reference LEDs by using a compact goniophotometer,” *MAPAN-JMSI* **24**, 143–152 (2009).

[23] P. Hanselaer, A. Keppens, S. Forment, W.R. Ryckaert, and G. Deconinck, “A new integrating sphere design for spectral radiant flux determination of light-emitting diodes,” *Meas. Sci. Technol.* **20**, 095111 (2009).

[24] European Commission, “Directive 2009/125/EC of the European Parliament and of the Council,” *Official Journal of the European Union* **L 285**, 10–35 (2009).

[25] J. Jakovenko, J. Formánek, V. Janíček, M. Husák, and R. Werkhoven, “High power solid state retrofit lamp thermal characterization and modeling,” *Radioengineering* **21**, 225–230 (2012).

[26] P. Vitta, P. Pobedinskas, and A. Žukauskas, “Phosphor thermometry in white light-emitting diodes,” *IEEE Photon. Tech. Lett.* **19**, 399–401 (2007).

[27] J. Hu, L Yang, and M.W. Shin, “Electrical, optical and thermal degradation of high power GaN/InGaN light-emitting diodes,” *J. Phys. D*: *Appl. Phys.* **41**, 035107 (2008).

[28] A. Christensen and S. Graham, ”Thermal effects in packaging high power light emitting diode arrays,” *Appl. Therm. Eng.* **29**, 364–371 (2009).

[29] H. Van der Broeck, G. Sauerländer, and M. Wendt, “Power driver topologies and control schemes for LEDs,” Proc. IEEE Applied Power Electronics Conference, Anaheim, USA, 1319–1325 (2007).

[30] Z. Ye, F. Greenfeld, and Z. Liang, "A topology study of single-phase offline AC/DC converters for high brightness white LED lighting with power factor pre-regulation and brightness dimmable feature," Proc. IEEE 34th Industrial Electronics Conference, Orlando, USA, 1961–1967 (2008).

[31] L. Gu, X. Ruan, M. Xu, and K. Yao, "Means of Eliminating Electrolytic Capacitor in AC/DC Power Supplies for LED Lightings," IEEE Trans. Power Electronics **24**, 1399–1408 (2009).

[32] H.M. Jung, J.H. Kim, B.K. Lee, and D.W. Yoo, "A New PWM dimmer using two active switches for AC LED lamp," Proc. IEEE Power Electronics Conference, Sapporo, Japan, 1547–1551 (2010).

[33] CIE 69, *Methods of characterizing illuminance meters and luminance meters* (Commission Internationale de l'Eclairage, Vienna, Austria, 1987).

[34] ISO, *Guide to the Expression of Uncertainty in Measurement (GUM)*, ISBN 92-67-10188-9 (1995).

[35] Y. Ohno, "A numerical method for color uncertainty," Proc. CIE Expert Symposium on Uncertainty Evaluation, Vienna, Italy, 8−11 (2001).

[36] U. Krüger and G. Sauter, "Comparison of methods for indicating the measurement uncertainty of integral parameters on the basis of spectral data by means of the measurement uncertainty of the f_1' value," Proc. CIE 2nd Expert Symposium on Measurement Uncertainty, Braunschweig, Germany, 159−163 (2006).

[37] S. Winter and A. Sperling, "Uncertainty analysis of a photometer calibration at the DSR setup of the PTB," Proc. CIE 2nd Expert Symposium on Measurement Uncertainty, Braunschweig, Germany, 139−142 (2006).

[38] E. Ikonen, T. Poikonen, P. Kärhä, P. Manninen, and F. Manoocheri, "Determination of f_1' and its uncertainty with biased and random error models," Proc. CIE Expert Symposium on advances in photometry and colorimetry, Turin, Italy, 55–60 (2008).

[39] Y. Ohno, "Detector-based luminous-flux calibration using the absolute integrating-sphere method," *Metrologia* **35**, 473–78 (1998).

[40] J. Hovila, P. Toivanen, and E. Ikonen, "Realization of the unit of luminous flux at the HUT using the absolute integrating-sphere method," *Metrologia* **41**, 407–413 (2004).

[41] Y.W. Kim, D.H. Lee, S.N. Park, M.Y. Jeon, and S. Park, "Realization and validation of the detector-based absolute integrating sphere method for luminous-flux measurement at KRISS," *Metrologia* **49**, 273–282 (2012).

[42] K. Lahti, J. Hovila, P. Toivanen, E. Vahala, I. Tittonen, and E. Ikonen "Realization of the luminous-flux unit using an LED scanner for the absolute integrating-sphere method," *Metrologia* **37**, 595–598 (2000).

[43] S. Winter, M. Lindemann, W. Jordan, U. Binder, and M. Anokhin, "Convenient integrating sphere scanner for accurate luminous flux measurements," *Metrologia* **46**, S248–S251 (2009).

[44] Y. Ohno, M. Lindemann, and G. Sauter, “Analysis of integrating sphere errors for lamps having different angular intensity distributions,” *J. IES* **26**, 107–114 (1997).

[45] F. Manoocheri, P. Kärhä, L. Palva, P. Toivanen, A. Haapalinna, and E. Ikonen, “Characterisation of optical detectors using high-accuracy instruments,” *Anal. Chim. Acta* **380**, 327–337 (1999).

[46] S.W. Brown, G.P. Eppeldauer, and K.R. Lykke, “NIST facility for spectral irradiance and radiance responsivity calibrations with uniform sources,” *Metrologia* **37**, 579–582 (2000).

[47] M. Schuster, S. Nevas, A. Sperling, and S. Völker, “Spectral calibration of radiometric detectors using tunable laser sources,” *Appl. Opt.* **51**, 1950–1961 (2012).

[48] J. Hovila, M. Mustonen, P. Kärhä, and E. Ikonen, “Determination of the diffuser reference plane for accurate illuminance responsivity calibrations,” *Appl. Opt.* **44**, 5894–5898 (2005).

[49] P. Manninen, J. Hovila, L. Seppälä, P. Kärhä, L. Ylianttila, and E. Ikonen, “Determination of distance offsets of diffusers for accurate radiometric measurements,” *Metrologia* **43**, S120–S124 (2006).

[50] P. Manninen, P. Kärhä, and E. Ikonen, “Determining the irradiance signal from an asymmetric source with directional detectors: application to calibrations of radiometers with diffusers,” *Appl. Opt.* **47**, 4714–4722 (2008).

[51] P. Manninen, T. Koskela, L. Ylianttila, P. Kärhä, and E. Ikonen, “Estimation of the optical receiving plane positions of solar spectroradiometers with spherical diffusers on the basis of spatial responsivity data,” *Opt. Lett.* **34**, 3241–3243 (2009).

Aalto-DD 165/2012

ISBN 978-952-60-4901-4
ISBN 978-952-60-4902-1 (pdf)
ISSN-L 1799-4934
ISSN 1799-4934
ISSN 1799-4942 (pdf)

Aalto University
School of Electrical Engineering
Department of Signal Processing and Acoustics
www.aalto.fi

BUSINESS + ECONOMY

ART + DESIGN + ARCHITECTURE

SCIENCE + TECHNOLOGY

CROSSOVER

DOCTORAL DISSERTATIONS